J Mater Sci (2008) 43:4001–4008
DOI 10.1007/s10853-007-2395-y

REES RAWLINGS FESTSCHRIFT

Mechanical assessment of autogenous gas tungsten arc weldments of a super alpha-2 alloy

H. Abaszadeh · S. F. Kashani Bozorg

Received: 16 June 2007 / Accepted: 25 October 2007 / Published online: 3 April 2008

Abstract Butt welding of a 2-mm-thick super alpha-2 alloy (Ti-23Al-9Nb-2Mo-0.9Si) was carried out employing autogenous gas tungsten arc technique. Process parameters were adjusted to achieve full-penetration weld. Only β-Ti-based phase was detected in the fusion zone; however, minor quantities of a Ti_3Al-based structure were found at heat input higher than 518 J mm^{-1}. No cracking was observed within the fusion zone and its associated heat-affected zones. Subgrain boundaries and acicular transformation products were observed within the HAZ grains. The acicular transformation products are believed to be responsible for the higher microhardness value of the HAZ compared to those of the fusion zone and base material. It was found that the fusion zone and HAZ had lower strength and ductility than the base material. Fracture occurred within the HAZ, which is attributed to its higher microhardness value and acicular transformed microstructure. The maximum weld tensile strength achieved was about 90% of that of the base material.

Introduction

Super alpha-2 alloys are based on Ti_3Al titanium aluminide intermetallic compounds with β-phase-stabilizing elements such as Mo and V [1]. These alloys offer higher strength and ductility than the conventional alpha-2 alloys (e.g., Ti-24Al-11Nb, at. %) [2]. Kerry et al. showed the beneficial of Si addition to creep properties [3] and a class of modified super alpha-2 alloys has been developed [4]. These alloys have high-strength/weight ratios and are candidates for aerospace structural materials [5]. The joinability of these materials will be an important factor in determining their utilization.

Pulsed Nd:YAG [6] and continuous power CO_2 [7] laser beam welding studies on Ti-26Al-11Nb alpha-2 alloy demonstrated that full-penetration welds could be readily produced in 1.7-mm-thick sheet with no evidence of cracking. Also, David et al. [8] characterized electron beam welds in Ti-28Al-11Nb thin plate using a range of energy inputs to provide varying cooling rates and weld microstructures. Results obtained generally paralleled those of the lasers with a decrease in cooling rate. Moreover, Jicai et al. [9] and Wu et al. [10] reported the microstructure of the electron beam and laser-welded titanium aluminide-based alloy with higher Nb content, respectively. Acoff et al. [11] employed gas tungsten arc welding for joining near 0.5-mm-thick alpha-2 alloy. However, no detailed mechanical properties of the weldments have been reported in the literature.

The present paper deals with butt welding of a super alpha-2 alloy (Ti-23Al-9Nb-2Mo-0.9Si, all at. %) employing gas tungsten arc welding process. Also, mechanical assessment of the weldments is investigated.

Experimental procedure

A super alpha-2 alloy with the nominal composition of Ti-23at. %Al-9at. %Nb-2at. %Mo-0.9at. %Si was used as the base material for welding experiments. The alloy was cast, forged and heat treated in IMI Titanium Company [3]. Heat treatment experiment was conducted using solution treatment and quenching from the β-phase field and

H. Abaszadeh · S. F. Kashani Bozorg (✉)
School of Metallurgy and Materials Engineering,
Faculty of Engineering, University of Tehran,
P.O. Box 14395-553, Tehran, Iran
e-mail: fkashani@ut.ac.ir

Table 1 Welding process parameters and the related weld geometry

Weld No.	Current, A	Travel speed, mm/min
1	85	200
2	90	200
3	105	200
4	125	200
5	95	100
6	105	100
7	120	100
8	125	100
9	130	100
10	140	100

subsequent tempering at 800°C for one hour. Butt joints of 2-mm-thick coupons (45 × 30 mm) have been carried out employing an autogenous gas tungsten arc welding technique with a 3-mm-arc length at AC voltage of 15 V. Table 1 shows the applied welding process parameters. A copper block was used in the experimental arrangement set-up to obtain rapid weld cooling rates in this study. The samples were placed on the top of the copper block prior to welding. The following steps outline the procedures used to prepare the coupons before welding:

- The machined edges of each coupon were ground with 220-grit SiC paper to remove any burrs or edge cracks.
- The specimens were rinsed in acetone, dried and stored in sealed plastic bags. Prior to welding, each coupon was cleaned with acetone.

The coupons were welded while enclosed inside a Plexiglas chamber purged with high-purity argon (99.999%) due to reactivity of titanium with atmosphere. Argon was purged for 2 min prior to welding to displace any air in the shielding bag. The welded coupons were sectioned transversely and mounted in epoxy. Metallographic preparation involved grinding from 240-through 2000-grit SiC paper and polishing with 0.05-micron Al_2O_3 on cloth. Krolls reagent comprising 2-ml HF, 10-ml HNO_3 and 88-ml H_2O was used for etching the samples.

Inspection of the weldments was carried out using an X-ray fluoroscope model MU41. The microstructures of the base metal, heat affected and fusion zones were inspected using light and scanning electron (model Cam-Scan MV2300) microscopes. The former was linked with an energy dispersive spectrometer (EDS) for the determination of chemical analysis. The crystal structure of the base material and fusion zones was characterized using X-ray diffractometry (model Philips X'Pert Pro). Tensile testing was conducted on samples taken transversely to the sound weldments to evaluate the mechanical properties of the joints. The sizes of the tensile samples are shown in

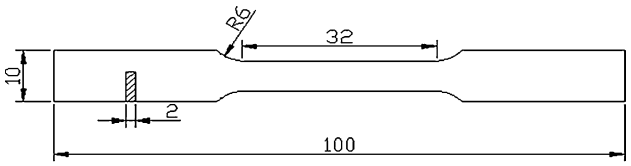

Fig. 1 Dimensions of the tensile samples, mm

Fig. 1. Testing temperature and speed were 27°C and 0.5 mm/min, respectively. Fracture surfaces of the tensile tested specimens were examined using scanning electron microscopy. Also, Vickers microhardness testing was carried out on mounted metallographic specimens using a 200 g load.

Results and discussion

Weld geometry and inspection

All weldments exhibited a metallic/silvery colour. The heat input was calculated using Eq. 1 [12]:

$$H_{\text{net}} = \eta \cdot \frac{V \cdot I}{S} \tag{1}$$

where H_{net} is heat input; η, process efficiency; V, voltage; I, current density and S, welding velocity. η is considered to be 0.48 for the gas tungsten arc process [13].

Table 2 shows that increasing heat input (increasing current or decreasing travel speed) resulted in increasing width and depth of the weldments.

Visual inspection of weldments did not reveal any cracks or other discontinuities. However, fluoroscopy examinations revealed minor porosities which decreased with increasing heat input. Sound weldments were produced using heat inputs of more than 518 J mm^{-1}.

Table 2 The calculated heat input and the measured width and depth of the weldments

Weld No.	Heat Input, J mm^{-1}	Penetration depth, mm	Weld width, mm
1	183	0.9	5.5
2	194	1.05	6.5
3	226	1.1	6.8
4	270	1.15	7.1
5	410	1.2	7.8
6	453	1.6	9.7
7	518	1.95	10.8
8	540	2	11.2
9	561	2	11.8
10	604	2	12.5

Microstructural characterization

The X-ray diffraction pattern of the base material is shown in Fig. 2. The reflections are consistent with the presence of the dominant Ti_3Al (alpha-2) and minor β-Ti-based crystal structures. Also, the backscattered electron micrograph (Fig. 3) revealed a two-phase Widmanstatten microstructure. The bright and dark contrasts are β and alpha-2 phases, respectively. Limited reflections with low intensities were detected which are thought to be related to O phase. This phase has been observed in relatively high-Nb content titanium aluminide alloys upon ageing and formed at the interface of β and alpha-2 phases [14].

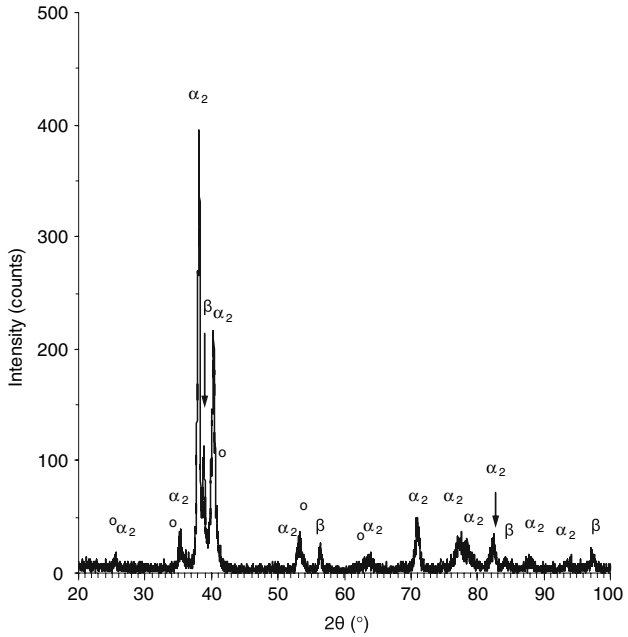

Fig. 2 X-ray diffraction pattern of the base material

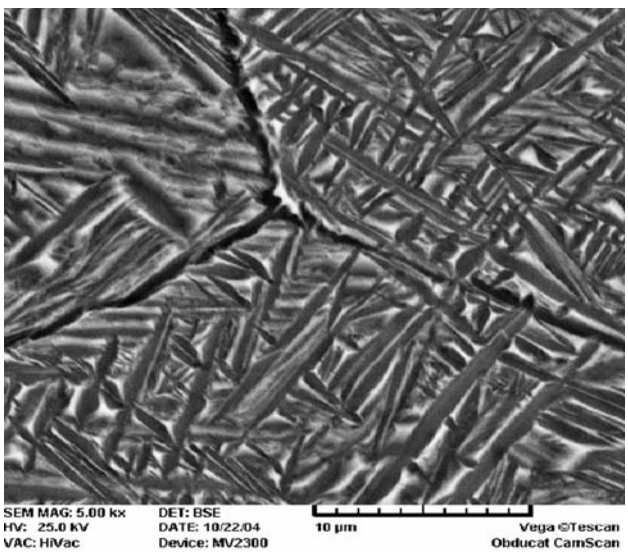

Fig. 3 Backscattered electron micrograph of the base material

Compared to the base material, the fusion zones and their associated heat-affected zones were more difficult to etch. Microstructure of the weld No. 6 is shown in Fig. 4. Coarse columnar grains have been revealed by optical microscopy. These grains were oriented perpendicular to the direction of the radial fusion boundary, which is the direction of the maximum temperature gradient and thus the maximum driving force for solidification. Also, a dendritic substructure could be observed within the grains. These characteristics paralleled those observed in typical titanium and titanium aluminide (alpha-2) alloy welds [9, 15]. The secondary arms of these dendrites show orthogonal angle with the main columnar ones, reflecting a cuboidal structure [16].

EDS area analysis revealed a decrease of Al content of up to 2% in the fusion zone. This decrease is believed to be due to evaporation and was found to be higher at the top of the weldments after using higher heat inputs (Table 3 and Fig. 5). Also, EDS point analysis showed substantial partitioning of Nb and Al to dendrites and interdendritic regions, respectively (not shown here).

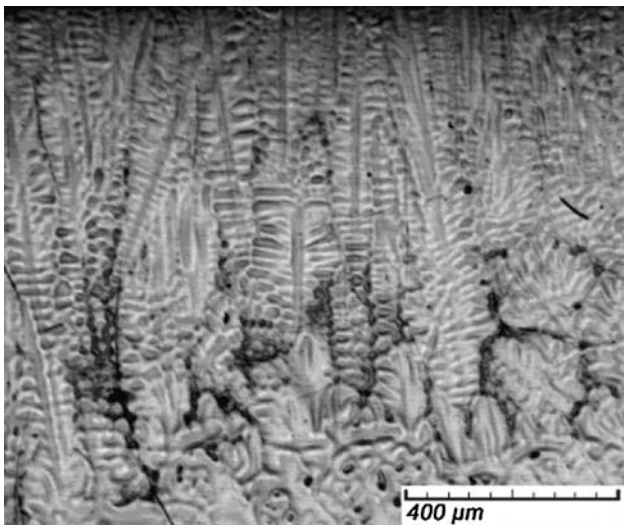

Fig. 4 Optical micrograph of the transverse section of the fusion zone showing coarse columnar grains with dendritic substructure

Table 3 EDS analysis of the top of the weld No. 9

Element	Weight%	Atomic%
Al	9.8	17.6
Si	1.2	2.1
Ti	69.1	70.0
Nb	15.4	8.0
Mo	4.5	2.3

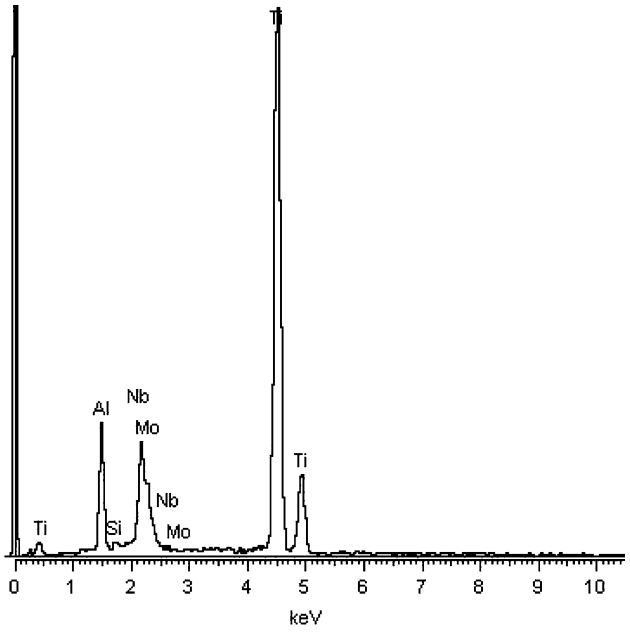

Fig. 5 X-ray spectrum of the top area of weld No. 9

Higher magnification revealed columnar grains which grew epitaxially upon coarse equiaxed grains of the HAZ towards the center of the fusion zone of weld No. 5 (Fig. 6). Coarsening of the microstructure was found after increasing the heat input.

X-ray diffraction patterns of the fusion zones consisted of limited peaks which were consistent with only the β structure. Figure 7 exhibits the X-ray diffraction patterns of the welds Nos. 3 and 5 produced at relatively low heat inputs (high cooling rates). Textures were affected by the temperature gradient. This suggests that the heat input plays an important role in the alignment of the fusion zone grains.

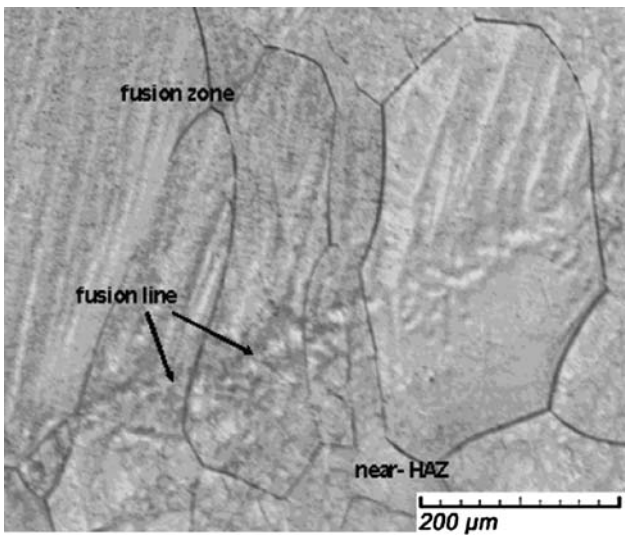

Fig. 6 Optical micrograph of the transverse section of the fusion/HAZ boundary exhibiting epitaxial growth

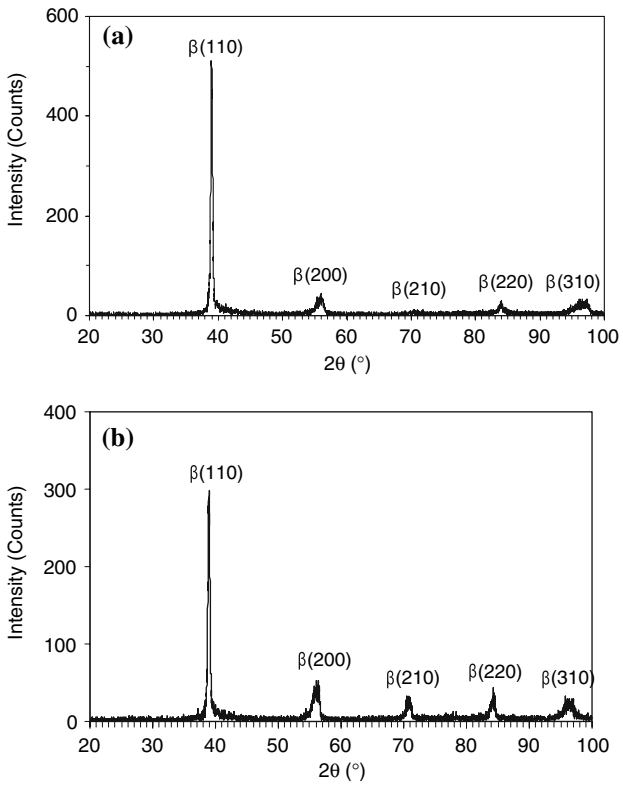

Fig. 7 X-ray diffraction patterns of the weld Nos. 3 (**a**) and 5 (**b**) produced using heat input of 226 and 410 mm^{-1}, respectively

Moreover, X-ray diffraction patterns of the weld produced at a heat input of more than 561 Jmm^{-1} exhibited extra reflections consistent with a Ti_3Al crystal structure (Fig. 8). It was reported earlier that the fusion zone microstructure of Ti_3Al-based alloys are sensitive to cooling rate

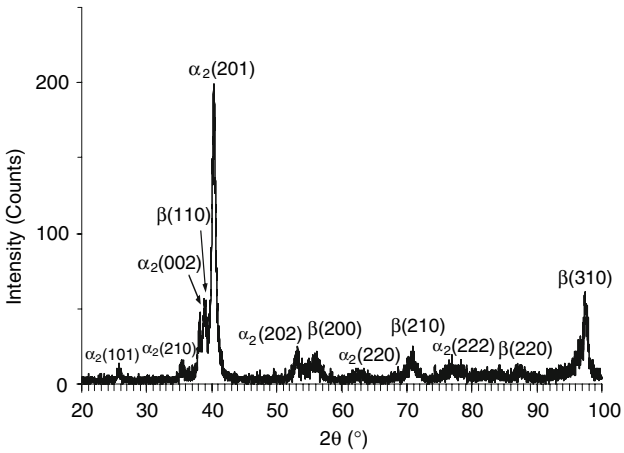

Fig. 8 *X*-ray diffraction pattern of weld No. 10 produced using heat input of 604 J mm^{-1}

[17]. Cieslak et al. [18] found only the transformed microstructure with no retained beta in the fusion zone of the gas tungsten arc welds of Ti-26Al-11Nb. Higher cooling rates may be achieved in the present investigation by using thicker plates (2 mm instead of 1.7 mm) or a copper backing plate.

Figure 9 shows the formation of subgrains within the HAZ indicative of the occurrence of a polygonization process. Away from the fusion zone (FZ)/heat-affected zone (HAZ) boundary, an acicular transformation product was observed within the HAZ grains (Fig. 10). EDS point analysis showed no difference in chemical composition within the HAZ grains between the matrix and acicular transformation products.

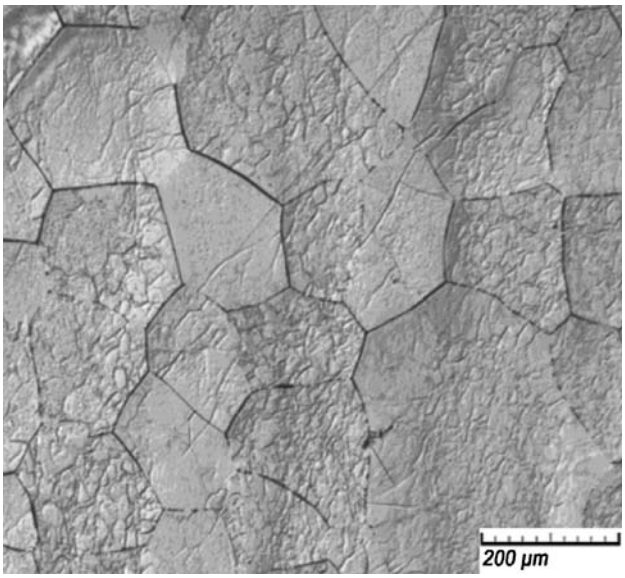

Fig. 9 HAZ grains with sub-boundaries

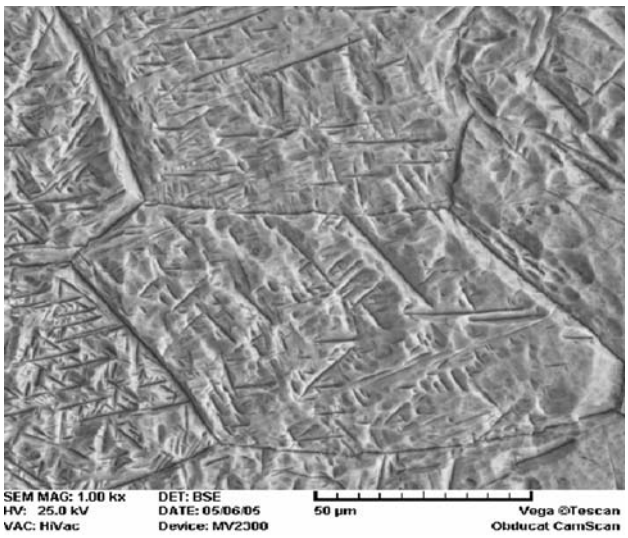

Fig. 10 Acicular products within the HAZ grains

Figure 11 exhibits microhardness profiles of two transverse sections of the weldments (welds Nos. 3 and 8). The average microhardness value of weld No. 8 (Fig. 11b) was slightly lower than that of weld No. 3 (Fig. 11a). This is attributed to more elemental partitioning in the interdendritic regions as the welding heat input was increased. Higher microhardness values were recorded for all the near heat-affected zones, compared to those of the fusion zones. It is believed that the increase in microhardness value is related to the formation of subgrains and transformation products within the HAZ grains. Also, it can be related to lower level of Al in the fusion zone due to evaporation. Microhardness value of the HAZ near the base material (in Fig. 11 described as 'Far-HAZ) decreases; this region remains relatively unaffected by welding thermal cycle.

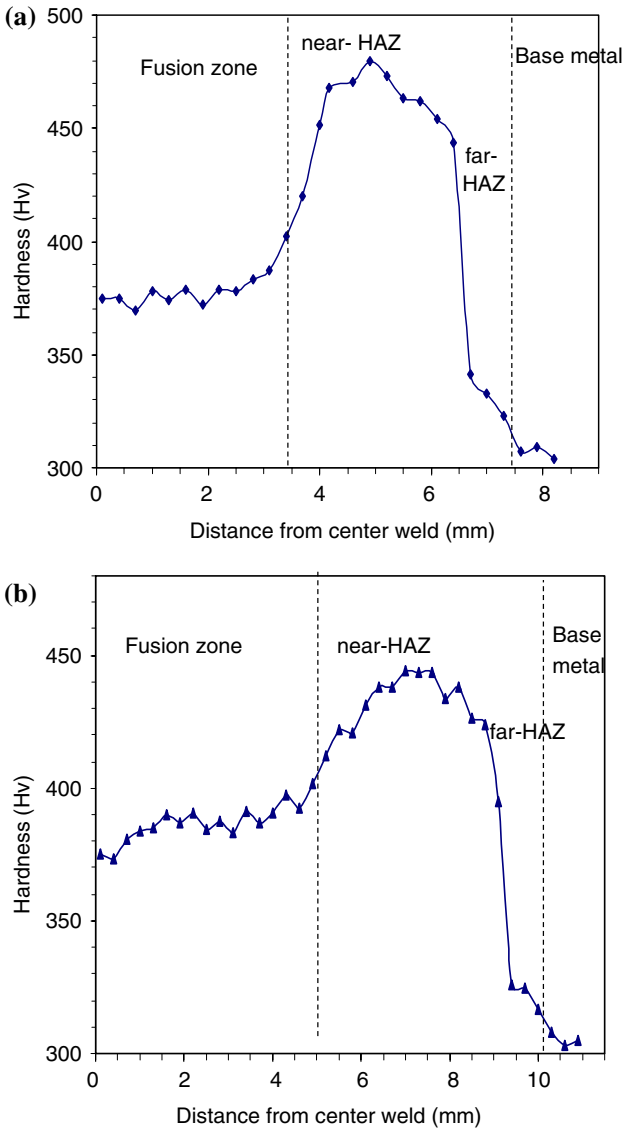

Fig. 11 Microhardness profiles of the weld Nos. 3 (**a**) and 8 (**b**) produced using heat input of 226 and 540 J mm^{-1}, respectively

Generally, the microhardness values obtained were found to be higher than those of Jicai et al. [9]. This may be attributed to the lower Al level of their base material.

Figure 12 shows the room temperature stress-strain curves of the tensile specimens taken from the substrate material and weld No. 8 (with full-penetration fusion zone), respectively. Tensile strength and ductility of the specimen taken from the weldments exhibited lower magnitudes compared to those of the base material. The results achieved from the tensile tests of sound weldments were in accordance with the results obtained from the microhardness tests (see Fig. 9). It is presumed that the reduction of mechanical properties (strength and ductility) is attributed to the formation of acicular products within the heat-affected zone.

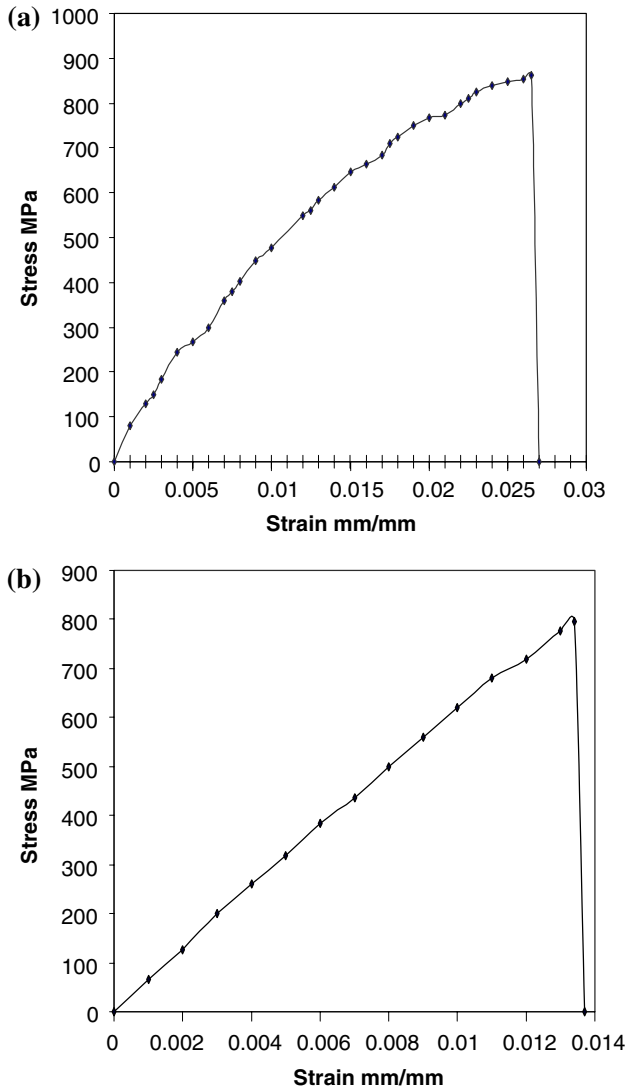

Fig. 12 Stress-strain curves for base material (**a**) and weld No. 8 (**b**) produced using heat input of 540 J mm^{-1}

Maximum weldment strength of 90% of that of the base material was achieved for the weld No. 8.

Tensile specimens taken from the sound weldments fractured in the heat-affected zone, very close to the fusion zone and those with minor porosities fractured in the fusion zone. Macroscopic examination of all fractured specimens showed shiny and faceted surfaces reflecting a cleavage fracture mode. Figure 13 exhibits fracture surface

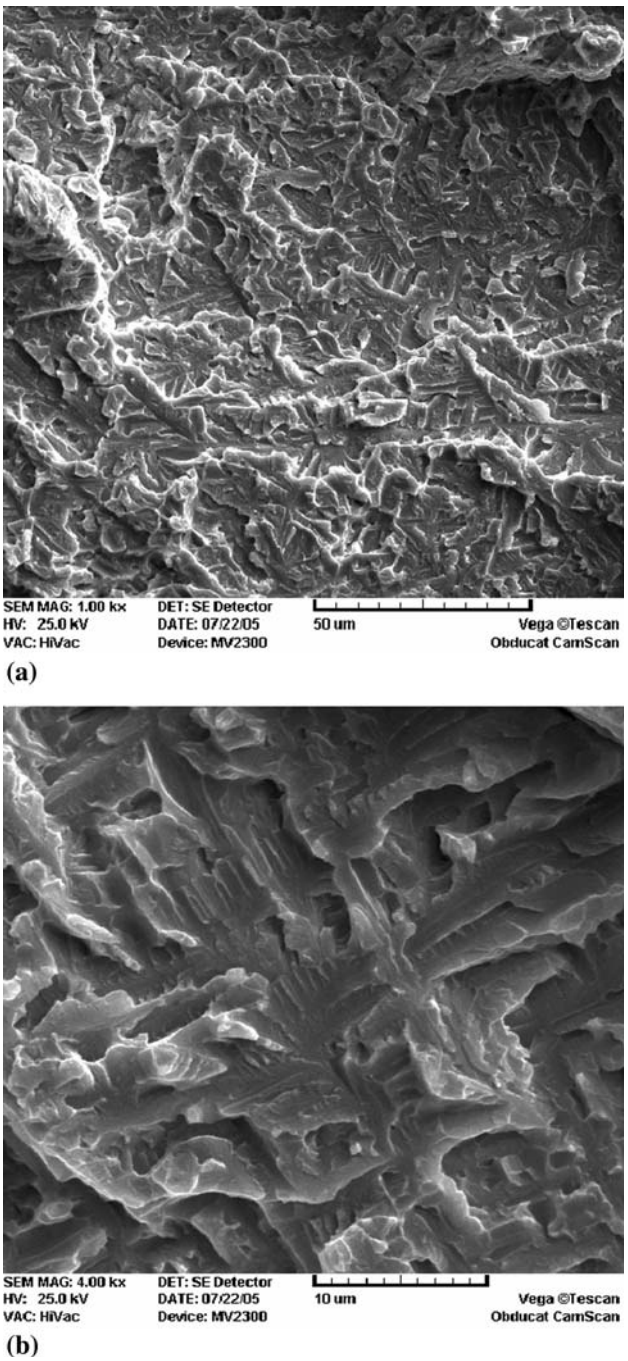

Fig. 13 Fracture surface of the base material exhibiting river pattern (**a**) and rosette features (**b**) employing higher magnification

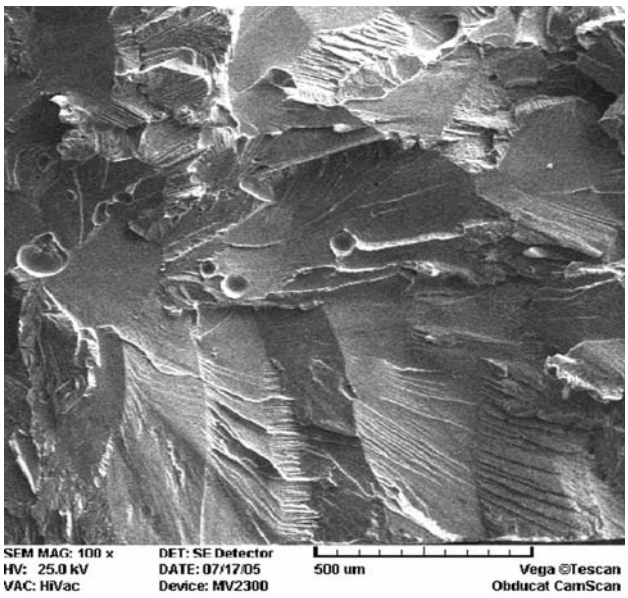

Fig. 14 Fracture surface of the tensile test specimen taken from the weld No. 5 exhibiting river pattern initiating from gas porosities

micrographs of the base material. A river pattern is observed (Fig. 13a) reflecting a cleavage fracture. Also, rosette-type features were observed at higher magnifications which is an indication of a quasi-cleavage fracture mode. Features were oriented similar to Widmansttatten microstructure of the base material.

SEM fractography of the weldment exhibited river patterns indicative of a transgranular cleavage fracture, which is common for the brittle materials (Figs. 14 and 15). The "river patterns" on each face are also typical of cleavage fracture. Small gas porosities were observed in the fracture surfaces of the weldments produced at relatively lower heat inputs. It is believed that gas entrapment within the fusion zone is due to relatively higher rate of solidification process.

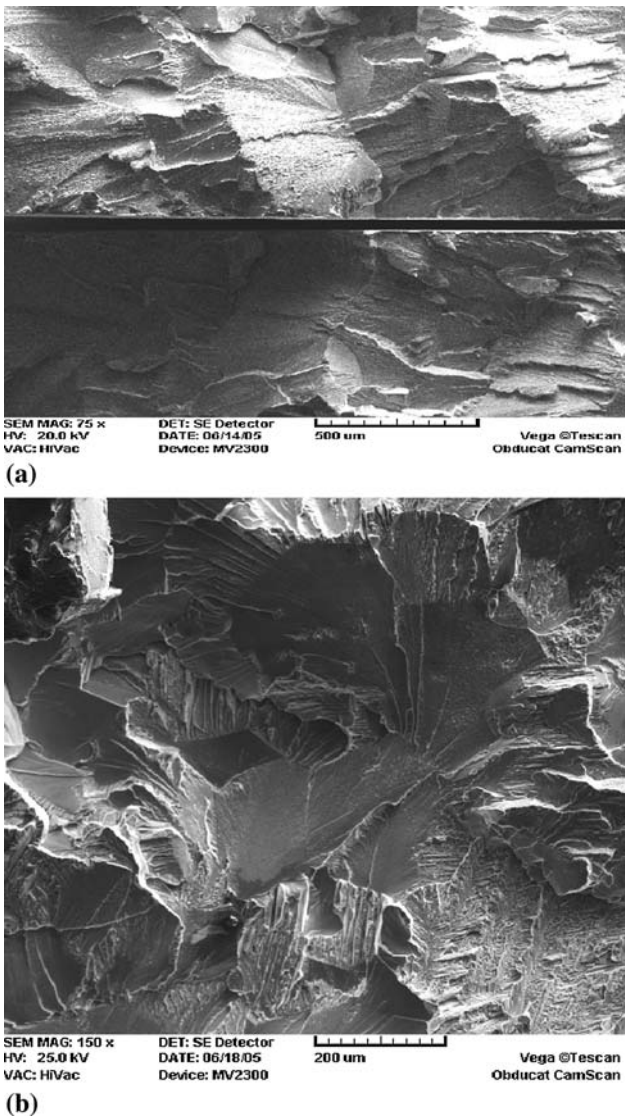

Fig. 15 Fracture surface of the tensile test specimen taken from the weld No. 8

Conclusions

1. Crack-free butt welding of a 2-mm-thick super alpha-2 plates has been achieved using tungsten inert gas technique.
2. The β-Ti (body centred cubic) crystal structure was obtained in the fusion zone. Subgrain and fine acicular transformation products were found in the heat-affected zone.
3. The average microhardness value of the fusion and heat-affected zones was shown to be higher than that of the base material. The highest microhardness value was found in the heat-affected zone.
4. The fusion zone and its associated heat-affected zones exhibited lower strength and ductility than the base material. The maximum strength obtained in the fusion zone was about 90% of that of the base material.
5. Fracture occurred in the heat-affected zone near the HAZ/weld boundary of the sound weldments produced at relatively high-heat inputs and was shown to be of transgranular cleavage type. This is attributed to the acicular transformation product of the high-temperature β-Ti-based phase.
6. Small gas pores were found to be a problem in the weldments produced using relatively low-heat inputs.

Acknowledgement Thanks are to Dr. S. Kerry of DRA Farnborough, England, for providing the base material and to University of Tehran for financial support for the present research.

References

1. Ward CH, Chand SJ, Balsone (1991) In: Kim YW, Boyer RR (eds) Microstructure/property relationships in titanium aluminides and alloys. The Minerals, Metals and Materials Society, pp 373
2. Ward CH (1993) Int Mater Rev 38(2):79rf
3. Kerry S, Winstone MR (1995) Mat Sci Eng A 192/193:856
4. Kerry S et al (1993) United States Patent 5,183,635, Titanium Alloys
5. Kim YW, Froes FH (1990) In: Whange SH et al (eds) High temperature aluminides and intermetallics. TMS, pp 465
6. Baeslack WA III, Cieslak MJ, Headley TJ (1988) Scripta Met 22:1155
7. Martin GS, Albright CE, Jones TA (1995) Weld Res Suppl 77s–82s
8. David SA, Horton JA, Goodwin GM, Phillips DH, Reed RW (1990) Weld J 69:133s
9. Jicai F, Huiqiang W, Jingshan H, Bingang Z (2005) Mater Char 54:99
10. Wu AP, Zou GS, Ren JL, Zhang HJ, Wang GQ, Liu X, Xie MR (2002) Intermetallics 10:647
11. Acoff VL, Thompson RG, Griffin RD, Radhakrishnan B (1992) Mat Sci Eng A152:304
12. ASM Handbook (1993) Weld Braz Solder 6:12
13. Mridha S, Ng BS (1999) Surf Eng 15:210
14. Banerjee D, Gogia AK, Nandi TK, Joshi VA (1998) Acta Metal 36(4):871
15. Baeslack WA III, Becker DW, Froes FH (1984) J Metal 36(5):46
16. Easterling K (1992) In: Butterworth-Heinemann (ed) Introduction to the physical metallurgy of welding, 2nd Oxford, p 82
17. Baeslack WA III, Broderick T (1990) Effect of cooling rate on the structure and hardness of a Ti–26 at.%Al–10 at.%Nb–3 at.% V–1 at.% Mo titanium aluminide. Scr Metall 24(2):319
18. Cieslack MMJ, Headley WA, Baeslack TJ III (1990) Met Trans A 21A:1273